ELSEVIER

International Journal of Heat and Fluid Flow 23 (2002) 700–709

International Journal of HEAT AND FLUID FLOW

www.elsevier.com/locate/ijhff

Experimental study on drag-reducing channel flow with surfactant additives—spatial structure of turbulence investigated by PIV system

Yasuo Kawaguchi [a,*], Takehiko Segawa [a], Ziping Feng [a,b,1], Peiwen Li [c]

[a] National Institute of Advanced Industrial Science and Technology, 1-2-1 Namiki, 305-8564 Tsukuba, Japan
[b] Center for Smart Control of Turbulence, 6-38-1 Shinkawa, Mitaka, 181-0004 Tokyo, Japan
[c] Department of Mechanical Engineering, Kyoto University, Yoshida Honmachi, 606-8501 Kyoto, Japan

Abstract

The turbulent frictional drag of water can be reduced dramatically by adding small amounts of drag-reducing materials, such as polymers or surfactants. As a percentage drag reduction of 80% can easily be achieved, this technique is thought to be the most practical method of reducing turbulent frictional drag. In this work, a double pulse particle image velocimetry (PIV) system was used to clarify the spatial velocity distribution of surfactant solution flow in a two-dimensional channel. A type of cationic surfactant cetyltrimethyl ammonium chloride ($C_{16}H_{33}N(CH_3)_3Cl$) mixed with the same weight of counter-ion material NaSal (HOC_6H_4COONa) was used as a drag-reducing additive to water at a mass concentration of 40 ppm. Instantaneous velocity distribution taken by PIV was examined to clarify the effect of surfactant. It was found that the instantaneous velocity distribution taken in water flow exhibits penetration from the low-speed fluid region into the high-speed region, which is one of the important events of turbulence energy production and turbulent mixing. Although this structure is commonly observed in water flow, it was not found in drag-reducing flow under the same Reynolds number. The strong vorticity fluctuation near the wall also disappeared and the integral length scale in streamwise direction of turbulent fluctuation had a smaller value in surfactant solution flow.

Keywords: Turbulence; Channel flow; Drag reduction; Surfactant; Spatial structure; PIV

1. Introduction

Since the discovery of Toms' effect (Mysels, 1949; Toms, 1948), the reduction of turbulent friction between a solid surface and fluid by adding drag-reducing materials has received increasing attention for saving the pumping power in fluid transportation. Polymers were initially used as drag-reducing additives for turbulent water flow to reduce the frictional drag by up to 80%. One successful application of drag reduction by adding polymers was that in the Trans-Alaska Pipeline, where the target discharge of one million barrels per day was obtained without having to construct additional pumping stations (Burger et al., 1982).

However, polymer solutions are strongly affected by mechanical degradation, which may result in shorter lifetime of drag reduction effectiveness. Surfactants were found in the last two decades also to reduce the frictional drag by 70–80% being less affected by mechanical degradation (Ohlendorf et al., 1986; Bewersdorff and Ohlendorf, 1988). Therefore, surfactants are now being considered as most practical drag-reducing additives to be used in the application. A recent application of the drag-reducing surfactant additives is to reduce the pumping power in the district heating and cooling systems where cationic surfactants are used in closed circuits (Gyr and Bewersdorff, 1995; Gasljevic and Matthys, 1996; Pollert et al., 1994). Although the environmental contamination arising from the minor toxic effect of surfactants may restrict their unlimited application in industry, for a closed circuit the effect on the environment can be minimized to an acceptable level.

The authors are continuing experimental studies on drag reduction phenomena in order to optimize the

* Corresponding author. Tel.: +81-298-61-7257; fax: +81-298-61-7275.
E-mail address: kawaguchi.y@aist.go.jp (Y. Kawaguchi).
[1] Present address: Daikin Air Conditioning Engineering Laboratory Ltd., 1304 Kaneokacho 591-8511 Sakai, Japan.

0142-727X/02/$ - see front matter
PII: S0142-727X(02)00166-2

Nomenclature

H	channel height
i	index for x-directional grid in PIV (particle image velocimetry, PIV) image
j	index for y-directional grid in PIV image
k	index for plane of PIV image
L	integral length scale given by Eq. (2)
Re	Reynolds number based on channel height H and bulk velocity U_b
R_{uu}	autocorrelation function given by Eq. (1)
S_{ij}	strain tensor
T_R	Trouton ratio
U	instantaneous velocity component in x-direction
$\overline{U}$	mean velocity based on the ensemble average
U_b	bulk mean velocity
u	velocity fluctuation component in x-direction
u'	RMS intensity of velocity fluctuation based on the ensemble average
u_τ	frictional velocity
$\overline{uv}$	kinetic Reynolds shear stress based on the ensemble average
V	instantaneous velocity component in y-direction
v'	RMS intensity of velocity fluctuation v based on the ensemble average
v	velocity fluctuation component in y-direction
W	channel width
w'	RMS intensity of velocity fluctuation w
x, y, z	spatial coordinate
Greeks	
η	shear viscosity
η_e	extentional viscosity
ν	kinetic viscosity
Σ	invaliant parameter
ω	vorticity
Ω_{ij}	vorticity tensor

district heating/cooling systems (Kawaguchi et al. 1996a,b, 1997a,b; Li et al. 2000, 2001a,b). Kawaguchi et al. (1996a) carried out the investigation to see how the turbulent characteristics in a two-dimensional channel were modified by surfactant additives by using a two-component laser Doppler velocimetry (LDV) system, and discussed the effect of the surfactant concentration and Reynolds number. They found that the two components of turbulent intensity were suppressed but had a finite value. Surprisingly, Reynolds shear stress disappears in fully drag-reducing flow as a result of the decorrelation between the two components of velocity fluctuation.

As the surfactant solution flow exhibits a complicated dynamical and thermal response, hot-film or other intrusive methods are unsuitable for measuring flow characteristics. Although the LDV allows us to make accurate measurements, they are limited only to one point at a time. Therefore, little information on the spatial structure such as length scale of turbulence is revealed by LDV. In contrast, PIV gives spatial information instantaneously. For this reason, PIV was employed to investigate the structure of drag-reducing flow in this paper.

2. Experimental apparatus and procedure

2.1. Water channel

The present experiments are carried out in a closed loop fluid flow facility, which is shown in Fig. 1. As shown in Fig. 1, the system consists of reservoir tank

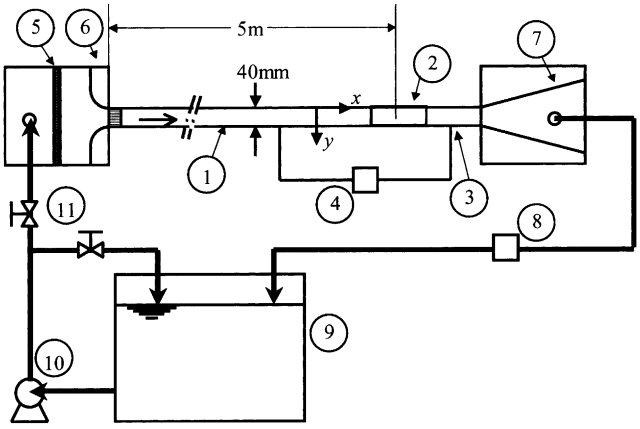

Fig. 1. Schematic diagram of two-dimensional water channel inner height: $H = 40$ mm, width: $W = 500$ mm. All the measurements were made at $x = 5000$ mm. (1) Two-dimensional channel, (2) window for PIV, (3) pressure tap, (4) pressure transducer, (5) filter, (6) contraction, (7) diffuser, (8) flowmeter, (9) tank, (10) pump, (11) valve.

(2.0 m^3), a pump, a settling chamber equipped with a nozzle, a two-dimensional channel, a diffuser and an electro-magnetic flowmeter. The test section is 40 mm high (H), 500 mm wide (W) and 6 m long (inside measurements). Most of the test section is made of transparent acrylic resin having thickness of 20 mm. The surfactant aqueous solution is circulated by the pump and supplied to the settling chamber. The chamber is equipped with a perforated pipe, stainless steel mesh and 1/12.5 contraction nozzle. At the entrance of the test section, a honeycomb of 150 mm length having 10 mm × 10 mm rectangular openings was used to remove large eddies. The PIV measurement position (L) is

5000 mm ($= 125H$) downstream from the inlet of the test section. For measurements of pressure drop, a high-precision differential pressure meter was used.

2.2. PIV system

The PIV measurement system consists of a double pulse laser, laser sheet optics, PIV camera, timing circuit, PC and software. The double pulse laser, (New wave Research Co. Ltd., MiniLase—II/20 Hz) is a combination of a pair of Nd-YAG lasers, each having an output of 25 mJ/pulse and repetition rate 20 Hz. By changing the combination of cylindrical lens, the laser sheet thickness can be modified in the range of 0.14–0.6 mm and beam spread angle can be switched in the range of 4.3–13.3°. The timing circuit (TSI Model 610032) communicates with the CCD camera and computer, and generates pulses to control the double pulse laser. The time duration of laser pulses is adjusted to give reasonable vector images. The interline CCD camera (PIVCAM 10-30, TSI Model 630046) used has a resolution of 1008×1018 pixels and can transfer images to the computer at the rate of 30 frames per second. A personal computer (Pentium II, 400 MHz) equipped with an image grabber board (TSI Model 600067) is used to control the whole system, picture frame acquisition and data processing using TSI's Insight ver. 2.01 software. The size of the interrogation area was set to 32×32 pixels and the size of overlap was 11 pixels, which corresponds to 34% of the size of the interrogation area. As the generation of error vector caused by imperfect condition of the optical system or software was unavoidable, a special Fortran program was written for eliminating the error vectors and performing statistical calculation based on the acquired vector distribution.

The arrangement of the water channel and PIV system is shown in Fig. 2. Cartesian coordinates are also shown in the diagram. According to the common usage, x, y and z coordinates are aligned to the streamwise, normal to the bottom wall and spanwise directions respectively. At the location of the measurements, the channel is equipped with two circular glass windows having aperture of 150 mm on the top and bottom walls of the channel. Two other glass windows, each with a rectangular opening of 200 mm in the x-direction by 60 mm in the y-direction, are installed on both sides of the channel. PIV image in the x–y plane are taken through the rectangular window from the z-direction. To allow this, a laser sheet aligned in the x–y plane is emitted from the top of the channel through the circular window. Most of the picture frames (40 mm × 34 mm) are taken to cover full height of the channel. In the most of the experiments, a series of 500 frames at the rate of 30 frames per second was taken. This means the velocity field was recorded in 15 Hz.

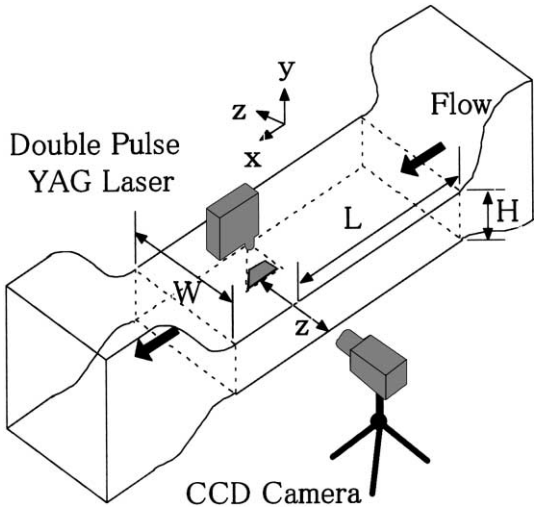

Fig. 2. Schematic view of PIV arrangement.

Fine particles of aluminum oxide were used for scattering particles, with nominal particle diameter of 5 μm. The concentration was carefully controlled to show clear PIV pictures.

2.3. Surfactant solution

The surfactant solution used in this study is cetyltrimethyl ammonium chloride (CTAC), which has the chemical formula of $C_{16}H_{33}N(CH_3)_3Cl$, dissolved in tap water. CTAC is a cationic surfactant that is known to be very effective for drag reduction when accompanied with suitable counter-ions. Cationic surfactants are less affected by calcium or sodium ions naturally found in tap water. This is the reason why cationic surfactants combined with a counter-ion such as sodium salicylate (NaSal, HOC_6H_4COONa) are frequently used in the basic studies or application to district heating and cooling systems.

For the surfactant drag-reducing additives, the rod-like micelle structure is thought to be the key to exhibit complicated rheological fluid properties including visco-elasticity. NaSal acts to reduce ion radius of CTAC to deform the micellar shape from globular to rod like. In this experiment, the same weight concentration of NaSal is always included in the CTAC solution. For the sake of simplicity, the solution of surfactant is designated as the surfactant concentration.

Prior to the channel experiment, the viscosity of the solution was measured by a rheometer with double wall Couette geometry (Rheometric Scientific F.E. Ltd., ARES 100FRTN1). At concentrations of 30 and 100 ppm, the shear viscosity of the solution at a shear rate of 200 s^{-1} in 25 °C was 0.82 and 0.97 mPa s respectively, and showed no stress thinning in the range of 10–300 s^{-1}.

3. Results and discussion

3.1. Effect of surfactant additives on friction factor and local mean velocity

The friction factor experimentally determined for water with and without surfactant additives is presented in Fig. 3. The friction factors are obtained by the static pressure distribution measurements along the channel. The Reynolds number was estimated from the bulk mean velocity U_b, channel height H and solvent kinematic viscosity v_0. The friction factor for water varies smoothly and obeys Dean's (1978) experimental formula for channel flow of Newtonian fluid. In contrast, the friction factor of the surfactant solution changes in a complicated way. It is observed that friction factor rises at $Re = 51{,}000$. This critical Reynolds number separates into two regimes. These regimes were previously called "complete drag reduction flow" and "post-drag reduction flow" by Kawaguchi et al. (1997b). The largest percentage of the drag reduction in this experiment was around 60%.

Mean velocity profile was determined based on the instantaneous velocity distribution taken by PIV. In each frame k, we can obtain two components of velocity U and V at grid points x_i and y_j. As the location of the grid point in each frame is fixed, we can define local mean velocity as the ensemble average $[\ ]_{k,i}$ through x_i and frame number k.

The mean velocity profile was determined based on 500 frames of the instantaneous velocity distribution taken by PIV. The obtained streamwise mean velocity profiles with and without surfactant are shown in Fig. 4, where lines represent the velocity profiles for water at each Reynolds number. Bulk mean velocity U_b was used for normalization. It is well known that the velocity profiles for water are roughly correlated by the $1/n$ power law. In this Reynolds number range, mean velocity near the centerline of the channel becomes flat and

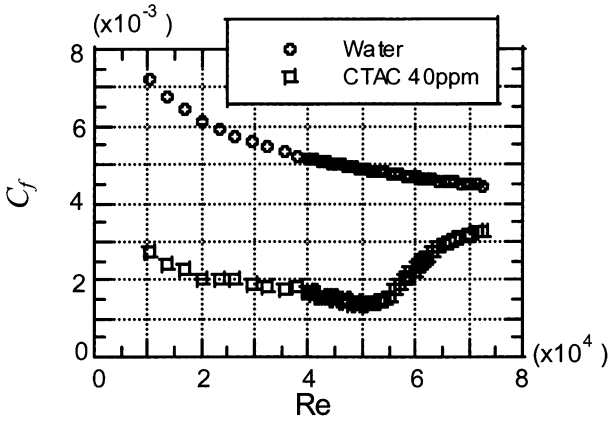

Fig. 3. Friction factor versus Re.

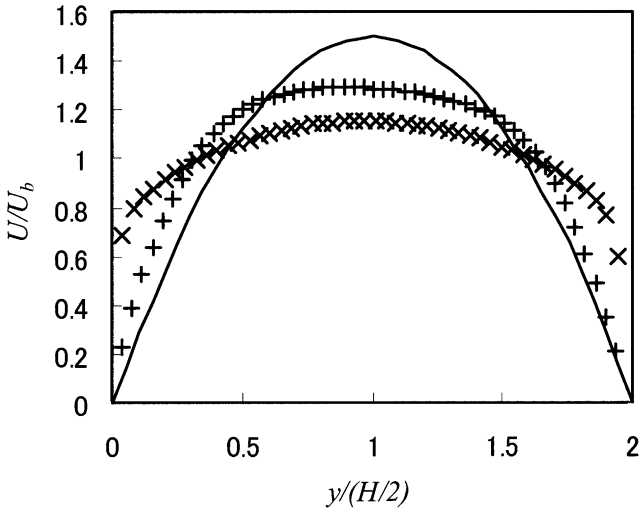

Fig. 4. Effect of surfactant additives on mean velocity profiles at $Re = 21{,}000$ (×: water, +: surfactant 40 ppm, for comparison, the laminar velocity profile is shown as a line).

the velocity gradient near the wall becomes large. In contrast, velocity profile for surfactant solution shows a steeper peak near the centerline, indicating that the mean velocity gradient near the wall of the surfactant solution is lower than that of the water flow. This finding corresponds to the result obtained by LDV (Kawaguchi et al., 1996a) that the velocity profile of drag-reducing flow approaches but does not coincide with laminar-like velocity profile.

The mean velocity profile falls between those of laminar and turbulent velocity profiles in Newtonian fluid flow. Recently, Saeki et al. (2000) made PTV measurements in drag-reducing flow in a pipe far downstream from the inlet and found some bi-modal characteristics where laminar flow and turbulent slug passed the pipe alternatively. This phenomenon is realistic because the some kind of surfactant solution is known to have much longer relaxation time. The authors also tried to detect the intermittent characteristics of the flow by PIV images. The 500 frames of velocity distribution were recorded and compared with each other. On our observation, drag-reducing velocity profile and weak turbulence intensity are observed in all figures. There is no clear evidence of intermittent nature of laminar and turbulent slug in our PIV images at $Re = 21{,}000$. One of the differences may be the surfactant concentration in the solution. Saeki et al. used 800 ppm of Ethoquad O/12 and 480 ppm of NaSal. These concentrations are 20 times larger than our present work, which uses 40 ppm of CTAC and NaSal. Trouton ratio T_R of fluid is defined by the extensional viscosity η_e divided by the shear viscosity η. For Newtonian fluid, T_R takes the value of three and for viscoelastic fluid such as surfactant or polymer solution, the ratio is known to

increase considerably. In addition to the large Trouton ratio, concentrated surfactant solutions have complicated rheological properties such as non-Newtonian shear viscosity, non-zero normal stress and large storage modulus. It is possible that these stress cause a different way to modify turbulence in the flow. Further discussion and investigation may be also necessary on this subject.

3.2. Effect of surfactant additives on statistical quantities of turbulent velocity fluctuation

Turbulent statistic quantities are defined by ensemble average of instantaneous local velocity U or/and V. Fig. 5 compares intensities of turbulent fluctuation normalized by frictional velocity u_τ. As previously reported in the study using LDV, turbulence fluctuations normalized by frictional velocity are not largely suppressed. The location of the peak in u' distribution shifts outward from the wall in the surfactant case. The distribution of v' shows that slight suppression occurs when surfactant is added to the water.

Fig. 6 shows the Reynolds shear stress $\overline{uv}$ profile in the water channel. The result is surprising because aside from the scatter in y of less than $y/H = 0.5$, the cross-correlation of u and v becomes almost zero in drag-reducing flow. As the two components of normal stress have finite values, the absence of Reynolds shear stress comes from de-correlation of the two components of velocity fluctuation.

3.3. Effect of surfactant additives on spatial distribution of instantaneous velocity distribution

First, instantaneous velocity distribution for water flow at $Re = 21{,}000$ is discussed. Fig. 7a shows a vector expression of spatial velocity distribution taken by PIV.

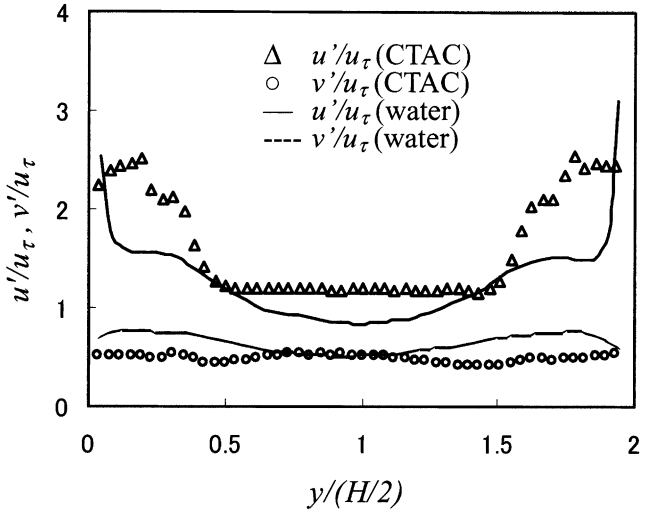

Fig. 5. Distribution of turbulent Intensities at $Re = 21{,}000$ (line: water, symbol: CTAC 40 ppm).

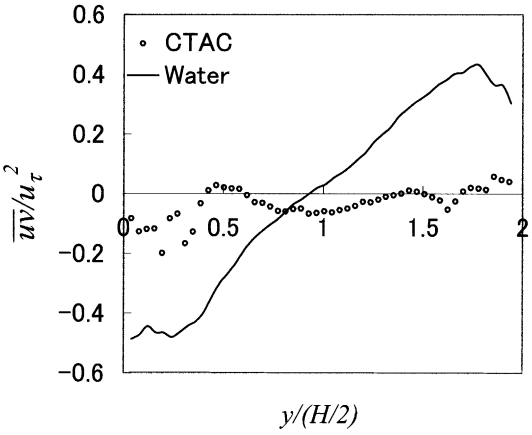

Fig. 6. Distribution of Reynolds shear stress at $Re = 21{,}000$ (line: water, symbol: CTAC 40 ppm).

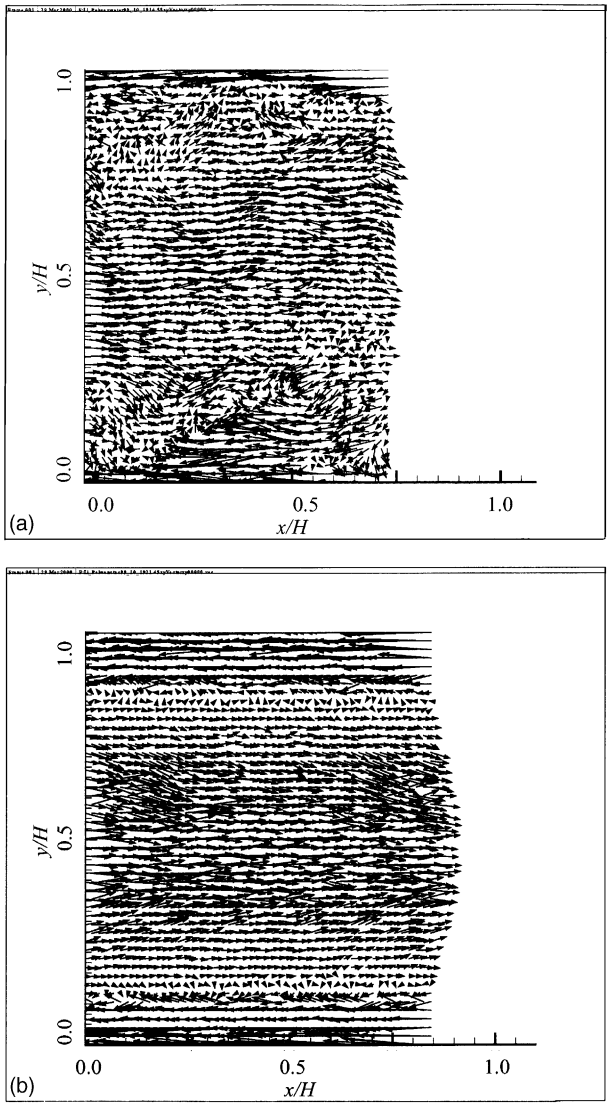

Fig. 7. Instantaneous velocity fluctuation vector in (a) water (CTAC 0 ppm), (b) drag-reducing flow (CTAC 40 ppm) at $Re = 21{,}000$.

In this figure, main flow direction is left to right and the frame covers height of the channel. In Fig. 7a, bulk mean velocity U_b is subtracted from all the vectors so that the vortex motion moving with U_b can be seen. This expression can be taken in a picture by a camera moving with the flow. So, the wall looks to move downstream direction at the speed of U_b.

Fig. 7a shows a velocity field composed of irregular direction as well as irregular magnitude of the velocity vectors. Generally, velocity vectors head to the right at the core region where y falls within 10–30 mm. In contrast with this, vectors locating closer than 5 mm from the wall head to the left. Between these regions, rotational eddy motion is clearly seen. The center location, size and magnitude are not uniform and the figure shows similar patterns of motion visualized by tracer in turbulent flow. Fig. 8a shows a contour map based on the magnitude of velocity. A random pattern of complicated

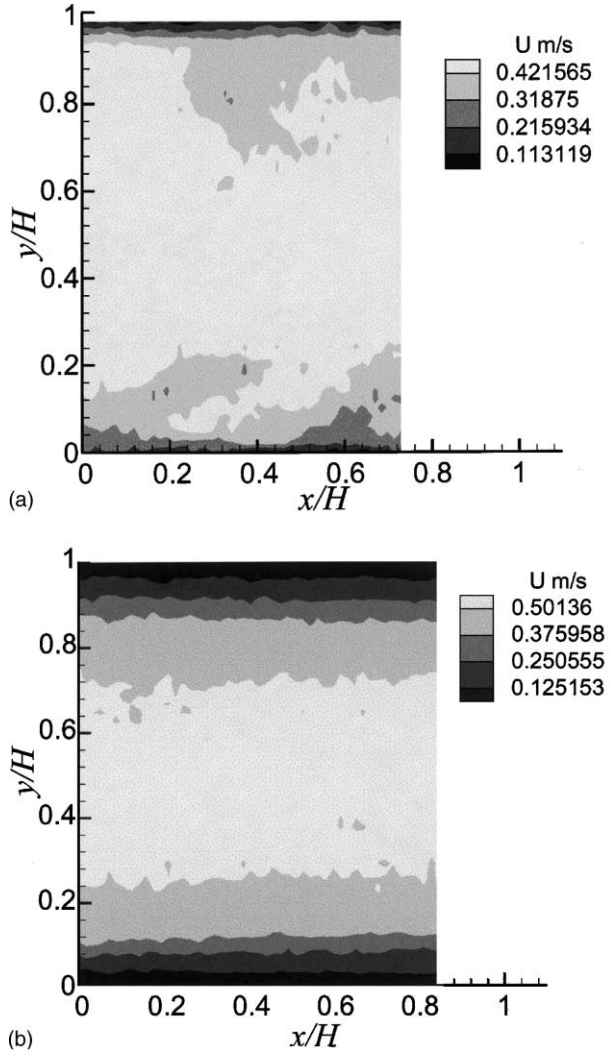

Fig. 8. Instantaneous velocity distribution in (a) water (CTAC 0 ppm), (b) drag-reducing flow (CTAC 40 ppm) at $Re = 21{,}000$.

ridge, valley and peaks can be seen in the middle of the channel. This means large velocity fluctuation in time and space occupies this field. In the region closer than $y/H = 0.1$ from the wall, contour lines are closely distributed. This comes from large velocity gradient near the wall commonly seen in turbulent wall flow. One interesting finding from the contour is the existence of acceleration or deceleration fronts near the wall. The acceleration front start from the location $(x/H, y/H) = (0.45, 0.02)$ and reaches to (0.6, 0.1), The front inclines downward and has angle of about 30° from the wall. Note that the mean flow direction in Fig. 8a is left to right. Another acceleration front appears at the location between (0, 0.04) and (0.25, 0.2). Deceleration front is not clear but can be seen between (0.15, 0.02) and (0.4, 0.2). These acceleration or deceleration fronts are a characteristic feature of the near wall turbulence. The turbulent structure accompanied with rapid acceleration or deceleration was investigated by VITA method applied to the hot wire record (Blackwelder and Kaplan, 1976; Johansson and Alfredsson, 1982). A study on spatial structure relating to turbulence control was also made based on the hot wire array probe (Kawaguchi et al., 1983).

Figs. 7b and 8b shows velocity field obtained in surfactant solution flow. Reynolds number is 21,000 and equal to the case for Figs. 7a and 8a. Figs. 7b and 8b show a vector and contour expression of spatial velocity distribution respectively. Bulk mean velocity U_b is subtracted from the vectors and as shown in Fig. 7b, the vortex motion is seen moving with U_b. Tilting angle of mean flow and each velocity vector are not always zero but much smaller than that in Fig. 7a. Weakly accelerated region can be seen in the core region but vortex motion cannot be clearly detected from this figure. Kawaguchi et al. (1996a) found that the dye streak in water flow at same Reynolds number was diffused by eddies having a variety of sizes. In contrast with this, dye streak in drag-reducing flow is much stable and slowly curved and it suggests diminishing of random motion of eddies. The present result given by PIV gives substance to the previous flow visualization study.

The contour lines shown in Fig. 8b run approximately parallel to the wall and its space is wider than the case in water flow in Fig. 8a. This comes from thickened shear layer and smaller velocity gradient near the wall.

The spatial pattern of the instantaneous velocity suggests that the large coherent motion in water flow disappears in surfactant solution flow. The lack of large-scale motion may affect the length scale of turbulent fluctuation. This scale is calculated by integrating the auto correlation function of turbulent fluctuation, i.e.

$$R_{uu}(\Delta x, y_j) = \frac{1}{u'^2}\left[\left\{U(x_i, y_j, k) - \overline{U}(y_j)\right\} \times \left\{U(x_i - \Delta x, y_j, k) - \overline{U}(y_j)\right\}\right]_{i,k} \quad (1)$$

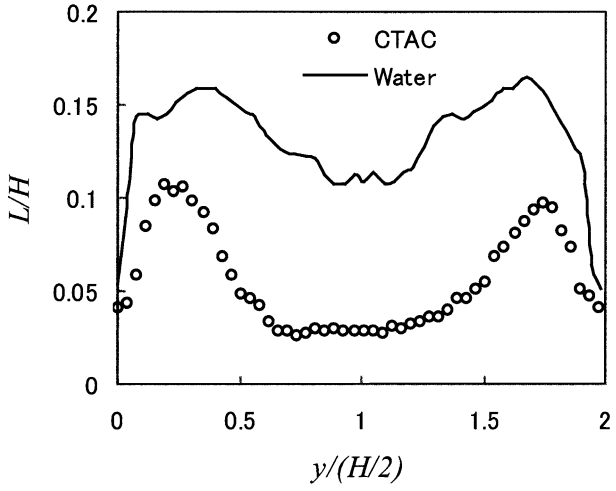

Fig. 9. Distribution of integral length scale of u' calculated in streamwise zone of h.

$$L(y_j) = \int R_{uu}(\Delta x, y_j)\,\mathrm{d}\Delta x \tag{2}$$

The integration area to calculate his length scale is one channel height h. As the longitudinal structure sometimes extends several times h, this calculated scale does not coincide with the integral length scale of turbulence. This zone limited length scale can be used to draw the information of the eddy size seen in the snapshot pictures like Fig. 7a and b. Fig. 9 shows the calculated result of the length scale based on the autocorrelation of u. The length scale L near the wall increases proportionally with the increase of y and it becomes around 0.12 of channel height H in the core region of the channel. In CTAC solution, the length scale is much smaller than that in water, thus supporting the idea of lower turbulent diffusivity and lower drag observed in surfactant solution flows.

3.4. Effect of surfactant additives on instantaneous spatial distribution of vorticity and flow structure classified by shear and vorticity tensor

Corresponding to the velocity fluctuation, vorticity fluctuation is also affected by surfactant additives. Fig. 10a and b compare vorticity fluctuation ω_z with and without surfactant additives, calculated from the common data demonstrated in Fig. 8a and b respectively. Note that contour lines are drawn to divide the range defined by minimum and maximum values appearing in the frame. These values are designated in each figure. As shown in Fig. 10a, the large positive and negative vorticities were observed around the observed front near the wall in Fig. 8a. In comparison, surfactant additives suppress violent vorticity motion as seen in Fig. 10b. Vorticity fluctuation is relatively weak and evenly distributed. The spatial scale of vorticity fluctuation seems

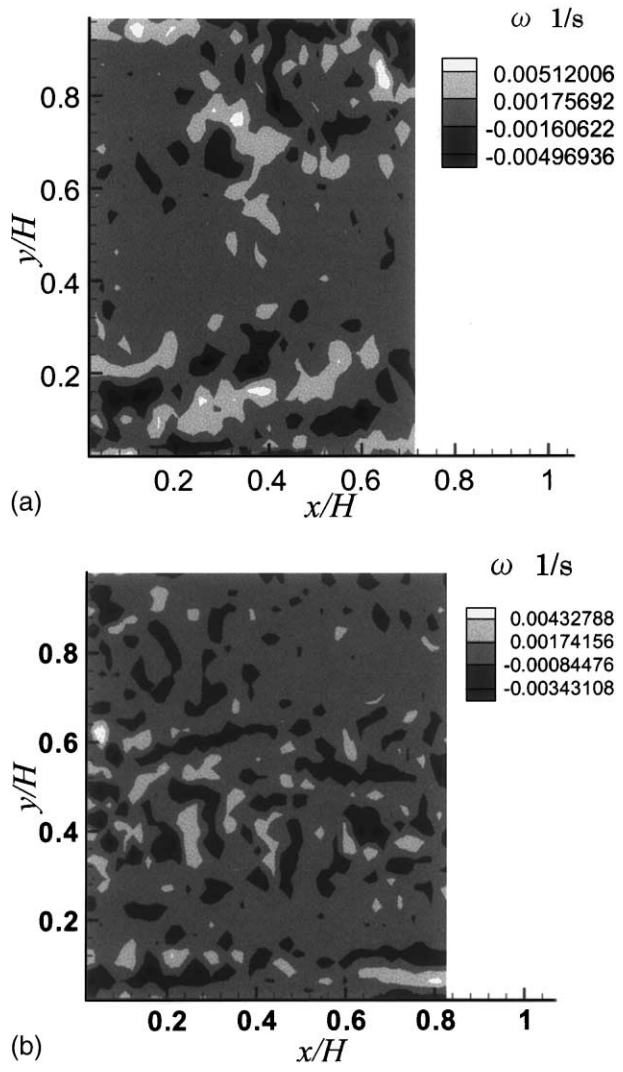

Fig. 10. Vorticity fluctuation distribution in (a) water flow (CTAC 0 ppm), (b) drag-reducing flow (CTAC 40 ppm) at $Re = 21{,}000$.

small and corresponds to smaller length scale as discussed in the previous section.

Kevlahan (1993) proposed the classification of turbulent structure based on the parameter $\Sigma = (S_{ij}^2 - \Omega_{ij}^2)/(S_{ij}^2 + \Omega_{ij}^2)$ where S_{ij} represents strain tensor and Ω_{ij} vorticity tensor. Kevlahan classified five basic structure types defined by the value of Σ and pressure. In this study, as the pressure is unknown, the following four types were determined based on Σ, S, Ω.

"Eddies": $|\Omega| > \Omega'$, $|\Sigma| > \Sigma'$ and $\Sigma < -1/3$,
"Shear": $|\Omega| > \Omega'$, $|\Sigma| > \Sigma'$ and $-1/3 < \Sigma < 1/3$,
"Convergence": $|\Omega| > \Omega'$, $|\Sigma| > \Sigma'$ and $\Sigma > 1/3$,
"Streaming": $|\Omega| < \Omega'$, $|\Sigma| < \Sigma'$ and $|u| > u'$

Primes on the symbols mean root mean square of the fluctuation. "Eddies" are regions of high vorticity, "Shear" structures are regions of shear strain, "Convergence" structures are regions of irrotational strain

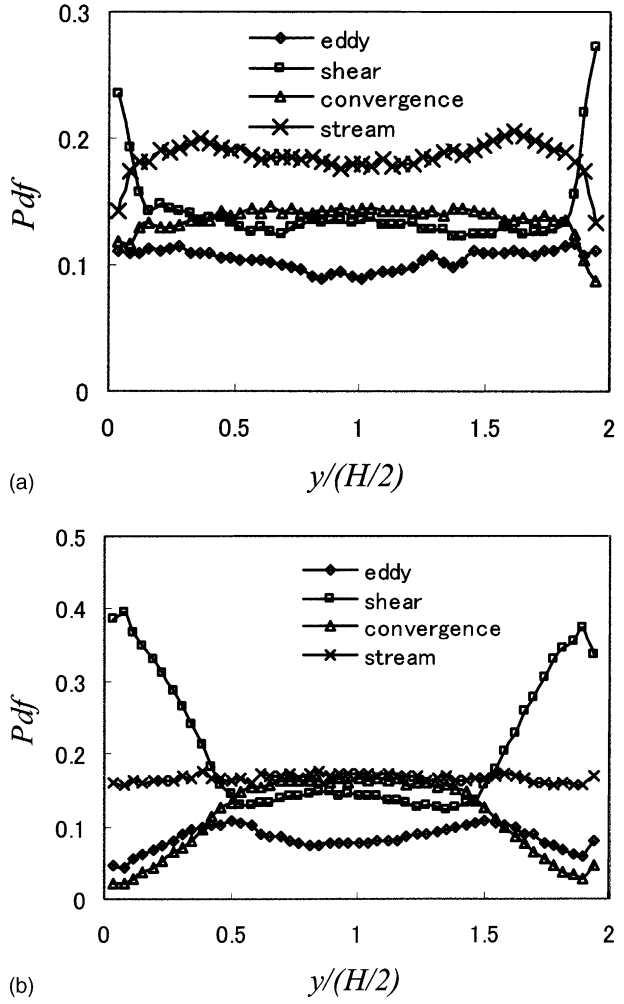

Fig. 11. Probability density function of classified structure in (a) water flow (CTAC 0 ppm), (b) drag-reducing flow (CTAC 40 ppm) at $Re = 21{,}000$.

characterized by converging streamlines, and "Streaming" structures are regions of low deformation and high kinetic energy. Kevlahan applied this classification to analyze the DNS result of distorting turbulence. This classification is also applicable to experimental data of PIV. Fig. 11a and b shows the distribution of probability of these four structures. In water channel flow shown in Fig. 11a, "Streaming" is the largest contributor in the most of the channel. Only in the thin layer near the wall, the probability of "Shear" structures becomes the largest. In contrast, surfactant solution flow has a thick layer characterized by "Shear" structures. In such layer, the probabilities of "Eddies" and "Convergence" structures become small.

4. Discussion

The reason and mechanism of drag reduction by additives are still under discussion because of the lack of experimental and analytical information. The major difficulties of experimental analysis in viscoelastic fluid flow are due to the fact that we cannot measure stress field which is independent of local strain rate of fluid. This is different from the analysis in Newtonian fluid flow, where the local stress can be estimated by local strain rate and viscosity.

In this paper, the authors are using the term of "turbulence" to name the fluctuating feature observed in drag-reducing flow but the situation is still not clear because there is conflicting evidence whether we judge the flow as turbulence or not. As observed in the previous section, the snapshot by PIV in drag-reducing flow is far from the turbulence in Newtonian fluid flow in high Reynolds number. But the following two characteristics suggest us that the similarity is present between the normal turbulence and drag-reducing flow.

(a) The shape of energy spectrum of velocity fluctuation becomes continuous and does not show dominant peak. This implies the presence of energy transfer process between the eddies having variety of scale. This cascade process characterizes the turbulence well.
(b) The drag-reducing state expands sometimes in a decade of Reynolds number range and seems to have common characteristics. In this range, we could not observe intermittent structure like a "turbulent bulge". This suggests that the drag-reducing state is different from unstable laminar flow in sub critical Reynolds number. But further careful investigations to find the similarity in terms of growth of randomness may be interesting and important.

The other reason of difficulties to classify present drag-reducing flow into laminar or turbulent is also coming from the difficulties to define "turbulence". But on the other hand, further investigation in drag reducing flow may give us a new insight which covers the "gray zone" between the stable laminar flow and normal turbulence.

4.1. Zero Reynolds shear stress

Then, we move to discuss the difference between the drag-reducing flow and normal turbulent flow. According to the result in Section 3.2, and LDV measurements by Kawaguchi et al. (1996a), in fully drag-reducing flow, both of turbulent intensities in two components u' and v' are suppressed but have finite value. The suppression ratio of y-directional components is much larger than the ratio of x-directional components. An astonishing fact is that Reynolds shear stress disappears in the whole range of the channel. Therefore, the correlation factor of two velocity components R_{uv} is completely zero in spite of the presence of

u' and v'. Kawaguchi et al. (1997b) also found that coherent structure detected by quadrant analysis shows no distinguished contribution from sweep or ejection. In other words, contributions from wallward and outward interaction are comparable to sweep and ejection.

In Newtonian fluid flow such as water, two components of velocity fluctuation usually have negative correlation in a shear layer. The idea of mixing length hypothesis is widely accepted to give a good approximation in such case. The idea contains random movements of fluid particles, to be mixed after certain time period. De-correlation of turbulence components in drag-reducing shear flow suggests that some of the idea in the mixing length theory is unsuitable. The free movements of fluid particles are inhibited in the drag-reducing state. In the case of Newtonian fluid flow in low Reynolds number, the shear stress caused by the strain prevents random motion of fluid element. In non-Newtonian viscoelastic fluid flow at high Reynolds number, the other force coming from elastic fluid property may suppressing free movement and mixing of the fluid element.

4.2. Production rate of turbulence

The investigations are still going on but force coming from the extensional viscosity can be one of the candidates for the suppressing force of turbulence production near the wall. Trouton ratio T_R is defined as the ratio of the extensional viscosity η_e and the shear viscosity η. All the low molecular weight fluid has Trouton ratio of 3 but some polymeric liquid has much larger values such as 10,000. Although all the drag-reducing fluid have complicated rheological properties, a large Trouton ratio is commonly found in drag-reducing fluid including dilute surfactant solution used in the present study. If we assume the high extensional viscosity, stretching motion of vortex will be inhibited and the production rate will be suppressed. At the same time, movement of the fluid must overcome the strong stretching resistance and discrepancy from the mixing length hypothesis becomes large.

In the Newtonian fluid turbulence, production rate of turbulence intensity is estimated by Reynolds stress multiplied by mean velocity gradient. In our observation, as the Reynolds shear stress is zero, the production rate also becomes zero. This conflicts with presence of turbulent intensities but we can imagine a different production process in viscoelastic fluid. As stated in the previous paragraph, the fluid strongly resists to stretching deformation in shear flow but at the same time, the fluid element stores energy in it. After moving to the other place, the elastic fluid element springs back and releases the energy and causes velocity fluctuation. The above explanation is qualitative and further estimation may be necessary in future but it gives a possible idea of turbulent production process in viscoelastic fluid flow.

4.3. Inhomogeneous turbulence suppression

Another aspect of drag reduction is inhomogeneous turbulence suppression, which means the y-directional component v' is much suppressed than x-directional one, u'. It can be also explained by large extensional viscosity. Due to the redistribution process, the excess energy in one directional component, such as u' is shared to other components v' and w'. As eddy-stretching motion is included in this process, when the extensional motion is resisted, the given energy to x-directional component does not redistribute to either the y- or x-directional component. This may explain the observation that v' is much more suppressed than u' in drag-reducing flow. This inhomogeneous suppression comes from the inhibition of energy transfer from u' to v' by large resistance of eddy stretching.

As the above qualitative explanation contains hypothetical idea, further investigations and efforts to quantitative estimation will be necessary in the future. One of the projects is accurate characterization of the drag-reducing solution by a sensitive Rheometer. The other one is direct simulation of non-Newtonian fluid turbulence containing reasonable constitutive equation.

5. Conclusions

The following conclusions were drawn from the present study.

1. The instantaneous velocity distribution taken in water flow exhibits penetration from the low-speed fluid region into the high-speed region, which is one of the important events of turbulence energy production and turbulent mixing. Although this structure is commonly observed in water flow, it was not found in drag-reducing flow under the same Reynolds number.
2. Turbulent normal stress u' and v' normalized with frictional velocity are not much suppressed by surfactant additives. Reynolds shear stress diappears in the whole range of the channel. This comes from de-coupling of two components of velocity fluctuation and corresponds to the diminishing of intense coherent motion near the wall.
3. The strong vorticity fluctuation near the wall disappears and the probabilities of ''Eddy'' and ''Convergence'' which accompanies vortex motion largely decrease near the wall.
4. Streamwise length scale integrated in area $h \times h$ has a smaller value in surfactant solution flow. This corresponds to smaller turbulent diffusivity in drag-reducing flow.

Acknowledgements

This research was carried out as a research project of the Center for Smart Control of Turbulence with the financial support by the Ministry of Education, Culture, Sports, Science and Technology (MECSST).

References

Bewersdorff, H.-W., Ohlendorf, D., 1988. The Behavior of drag-reducing cationic surfactant solutions. J. Colloid Polym. Sci. 266 (10), 941–953.

Blackwelder, R.F., Kaplan, R.E., 1976. On the wall structure of the turbulent boundary layer. J. Fluid Mech. 76 (1), 89.

Burger, E.D., Munk, W.R., Wahl, H.A., 1982. Flow Increase in the Trans-Alaska pipeline through use of a polymeric drag-reduction additive. J. Pet. Tech., 377–386.

Dean, R.B., 1978. Reynolds number dependency of skin friction and other bulk flow variables in two-dimensional rectangular duct flow. ASME J. Fluid Eng. 100, 215–223.

Gasljevic, K., Matthys, E.F., 1996. Field test of a drag-reducing surfactant additives in a hydraulic cooling system. ASME FED 237, 249–260.

Gyr, A., Bewersdorff, H.-W., 1995. Drag reduction of turbulent flows by additives. Kluwer Academic Publishers, The Netherlands.

Johansson, A.V., Alfredsson, P.H., 1982. On the structure of turbulent channel flow. J. Fluid Mech. 122, 295–314.

Kawaguchi, Y., Yano, T., Suzuki, K., 1983. An experimental study on coherent structure in a turbulent boundary layer disturbed by a cylinder. Proc. 8th Biennial Symp. Turbulence, Rolla, MO, USA.

Kawaguchi, Y., Tawaraya, Y., Yabe, A., Hishida, K., Maeda, M., 1996. A turbulent transport mechanism in a drag reducing flow with surfactant additive investigated by two component LDV. 8th Intl. Symp. Appl. Laser Tech. Fluid Mech., July 8–11, Lisbon, Portugal, II, 29.4.1–29.4.7.

Kawaguchi, Y., Tawaraya, Y., Yabe, A., Hishida, K., Maeda, M., 1996b. Active control of turbulent drag reduction in surfactant solutions by wall heating. ASME 1996 Fluid Eng. Div. Conf., July 7–11, San Diego, USA 2, 47–52.

Kawaguchi, Y., Daisaka, H., Yabe, A., Hishida, K., Maeda, M., 1997a. A Existence of Double Diffusivity Fluid Layers and Heat Transfer Characteristics in Drag Reducing Channel Flow, Turbulence, Heat and Mass Transfer. Delft University Press, The Netherlands, pp. 157–166.

Kawaguchi, Y., Daisaka, H., Yabe, A., Hishida, K., Maeda, M., 1997b. Turbulence characteristics in transition region of dilute surfactant drag reducing flows. In: Proc. 11th Intl. Symp. Turbulent Shear Flows, Sep. Grenoble, France, pp. P1-49–P1-54.

Kevlahan, N.K.-R., 1993. Rapid distortion of turbulent structures. Appl. Sci. Res. 51, 411–415.

Li, P.W., Kawaguchi, Y., Yabe, A., 2000. Feasibility Study of New Heat Transportation System with Drag-reducing Surfactant Additives, Proc. Symp. Energy Eng. 21st Century, January 9–13, HongKong, China, pp. 716–722.

Li, P.W., Kawaguchi, Y., Daisaka, H., Yabe, A., Hishida, K., Maeda, M., 2001a. Heat transfer enhancement to the drag-reducing flow of surfactant solution in two-dimensional channel with mesh-screen inserts at the inlet. ASME J. Heat Transf. 123, 779–789.

Li, P.W., Kawaguchi, Y., Yabe, A., 2001b. Transitional heat transfer and turbulent characteristics of drag-reducing flow through a contracted channel. J. Enhanced Heat Transf. 2001b (8), 23–39.

Mysels, K.J., 1949. Flow of Thickened Fluids, US Patent 2,492,173, December 27.

Ohlendorf, D., Interthal, W., Hoffmann, H., 1986. Surfactant systems for drag reduction: physico-chemical properties and rheological behavior. Rheol. Acta 25, 468–486.

Pollert, J., Zakin, J.L., Myska, J., Kratochivil, P., 1994. Use of friction reducing additives in district heating system field test at Kladno-Krocehlavy, Czech Republic. Proc. 85th Int. District Heating Cooling Assoc. Seattle, USA, pp. 141–156.

Saeki, T., DeGuzman, M.R., Morishima, H., Usui, H., Nishimura, T., 2000. A flow visualization study on the mechanism of turbulent drag reduction by surfactants. J. Soc. Rheol., Jpn. 28 (1), 35–40.

Toms, B.A., 1948. Some observation on the flow of linear polymer solutions through straight tubes at large Reynolds numbers. In: Proc. 1st Int. Cong. Rheol., vol. II. North Holland, Amsterdam, pp. 135–141.